

# Complementary TEM and AFM Force Spectroscopy to Characterize the Nanomechanical Properties of Nanoparticle Chain Aggregates

Weizhi Rong,<sup>†,§</sup> Andrew E. Pelling,<sup>‡,§</sup> Andrew Ryan,<sup>‡</sup> James K. Gimzewski,<sup>‡</sup> and Sheldon K. Friedlander<sup>\*,†</sup>

*Chemical Engineering Department and Department of Chemistry and Biochemistry, University of California, Los Angeles, Los Angeles, California 90095*

*Received August 4, 2004; Revised Manuscript Received September 23, 2004*

## ABSTRACT

Nanoparticle chain aggregates are used as reinforcing fillers in elastomers (rubber) and significantly enhance the mechanical properties (tensile strength, Young's modulus) of elastomers. Insight into mechanisms of the performance of nanoparticle chain aggregates can be obtained from force vs displacement (force spectroscopy) measurements made with an AFM tip and an aggregate-coated substrate. Distinctive sawtooth patterns were observed which were interpreted as aggregate stretching and breaking events. Based on the measurements, estimates of the aggregate nanomechanical properties were made.

Nanoparticle chain aggregates (NCAs) are branched structures composed of primary particles with diameters ranging from 1 to 50 nm. They form either during nanoparticle synthesis in aerosol reactors or in high-temperature combustion processes. Interest in NCAs stems from their importance in the manufacture of nanocomposite materials such as reinforced rubber<sup>1</sup> and their role in air pollution.<sup>2</sup> The use of NCAs as reinforcing fillers in rubber and other polymeric materials results in improved mechanical properties including increased tensile strength and Young's modulus.<sup>1</sup> Although fillers constitute a significant volume fraction (30–40%) of the nanocomposite, the mechanism of interaction between NCA and the polymer chains is not well understood.<sup>3–6</sup>

The scientific community has a deep understanding of polymer fundamentals and the ability to design polymer molecules with desired properties. In contrast, much less is known about NCA properties. However, recent studies have provided insight into the mechanisms behind NCA effects. For example, in the first study of its kind, Friedlander et al.<sup>7</sup> found what appeared to be elastic-like behavior of individual titania chains deposited on carbon/Formvar films on transmission electron microscope (TEM) grids. Pu et al.<sup>8</sup> found an enhancement in nanocomposite performance when silica nanoparticles were embedded in a polymer. The enhancement increased when the particles were aggregated. The results

are suggestive qualitatively, although the size and nature of the silica particle aggregates differed significantly from commercial reinforcing fillers usually generated by aerosol processes.

To conduct a better controlled study of the dynamics of chain stretching and contraction, Suh et al.<sup>9</sup> designed and built a novel nanostructure manipulation device (NSMD) which made it possible to apply tension to nanostructures mounted in the TEM. NSMD studies of stretching and contraction of such chains in the TEM were made under different maximum values of strain.<sup>10,11</sup> Stretching causes initially folded NCA to reorganize into a taut configuration. Further stretching either leads to chain breakage with fast recoil of the broken segments or to a partial elastic behavior of the chain at small strains.<sup>11</sup> This showed again the elastic nature of the NCA. However, important mechanical properties of NCAs, such as the tensile strength and Young's modulus, remain to be studied quantitatively.

This paper describes force vs displacement measurements of the interactions of an atomic force microscope<sup>12</sup> (AFM) tip with graphitic NCA deposited on a silicon substrate. AFM single molecule force spectroscopy (SMFS) has been employed to investigate the intramolecular forces within individual polymeric molecules, such as DNA<sup>13,14</sup> and proteins.<sup>15–17</sup> SMFS is an important development of atomic force microscopy. It extends AFM's capabilities to study the mechanics of inter- and intramolecular interaction with a precision in the piconewton (pN) range. SMFS relies on the force–distance curves obtained from a “fly-fishing” like

\* To whom correspondence should be addressed. E-mail: skf@ucla.edu.

<sup>†</sup> Chemical Engineering Department.

<sup>‡</sup> Department of Chemistry and Biochemistry.

<sup>§</sup> These authors contributed equally to the research described here.

approach where the tip of the cantilever catches single polymer chains immobilized at one end to a substrate. The process is usually automated. From the curves obtained, it is necessary to sort the data and classify the curves into meaningful pulling events. This often entails the analysis of several hundred to thousand force curves extracting those events that correspond to the pulling of a single molecular strand.

SMFS is well suited to single molecular chains. For instance, for single polymer chains of PMAA,<sup>18</sup> SMFS enabled the entropic elasticity to be determined and the data compared with entropic-based statistical mechanical, random walk models. Unfortunately, major problems arise when applying the technique to multiple polymer chains. The reason for the difficult analysis of multiple polymer chains is that force–distance curves typically recorded in SMFS rely on an analysis that assumes the data correspond to one single molecular chain being stretched between tip and surface. While double or triple chains might also be measured in the experiment, SMFS is not an imaging technique that enables the microscopic structure of the stretched polymer chain to be observed. Fortunately, in previous studies by Suh et al.<sup>10</sup> discussed above that employed a TEM and the NSMD, the morphology and general characteristics of the aggregate stretching process have been observed for the samples studied here (Figure 1a). Using these images as a general stretching model for the NCAs we are able to perform force spectroscopy measurements on the aggregates and interpret the results in light of their well-documented stretching and breaking process.

TEM nanostructure manipulation provides high resolution images of the NCA stretching and breaking process, and AFM force measurements are currently the best way to determine the dynamic and mechanical properties associated with this process on the nanoscale. Thus the two methods are complementary. In this study we report structural and mechanical data obtained from both methods. The results have application to the design of nanocomposite materials including elastomers,<sup>1</sup> the sampling and break-up of aggregates by high velocity impaction,<sup>19</sup> and, possibly, the fabrication of deformable electronic surfaces.<sup>20–22</sup>

Graphitic NCAs were generated by laser ablation (Figure 1b).<sup>23,24</sup> Targets composed of graphite (spectroscopic grade, Ted Pella Inc.) in the form of 2 mm thick disks, 25.4 mm in diameter, were ablated using a YAG laser (Hughes Aircraft Co., MDIVAD Laser Rangefinder) in an Ar atmosphere. The average laser power was about 100 mJ/pulse, with a pulse frequency of 10 Hz. The NCAs in the gas exiting the laser ablation chamber were deposited on a silicon substrate (0.5 mm in thickness and 1 cm × 2 cm in shape, Department of Physics, University of Karlsruhe) from the carrier gas, using a low-pressure single-stage impactor<sup>25</sup> with a nozzle diameter of 2 mm. The impactor was connected to a critical orifice with a throat area of about 0.01 mm<sup>2</sup> upstream and a vacuum pump (TRICAC D4B, Leybold Vacuum, Cologne, Germany) downstream. During ablation, which lasted for 10 s, the flow rates of the carrier gas into the ablation chamber and the impactor were 1 L/min and 0.27 L/min, respectively. The

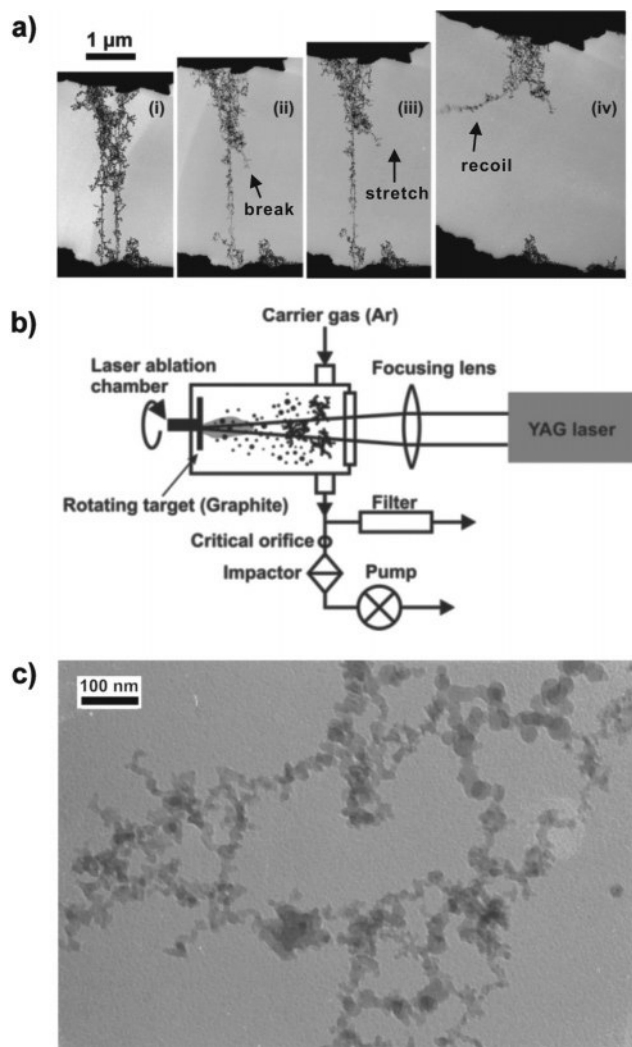


**Figure 1.** (a) TEM photo showing the sequential stretching and breaking of single NCA chains: (i) NCAs deposited between two separating surfaces,<sup>10,11</sup> (ii) stretching and breaking of one of the chains, (iii) stretching and (iv) breaking of the second chain. The lower broken part disappeared, probably because it recoiled to the specimen support. In both (ii) and (iv), the chain broke somewhere along its length and did not detach at the support surfaces. (b) Schematic diagram of the laser ablation system for generating NCAs. The rotating target was ablated by the laser beam, forming a vapor plume (gray area in the figure). (c) TEM image of graphitic aggregates generated by laser ablation. The average primary particle size is about 15 nm. The actual surface coatings were significantly denser than those shown in the figure.

impactor operated at a pressure of 5.5 mbar during deposition. The aggregate number concentration was about 10<sup>6</sup>/cm<sup>3</sup>, measured using a differential mobility analyzer (DMA) (TSI, St. Paul, model 3080) and condensation particle counter (CPC) (TSI model 3010).

Figure 1c shows graphitic aggregates deposited on a TEM grid. The photo was taken in a TEM (JEOL, model JEM-100 CX) operated at an accelerating voltage of 100 kV and a magnification of 100 000. The primary particle size was 10 to 30 nm and the length of the aggregates about 2 μm. The aggregates deposited on the silicon substrate formed a dark spot with a diameter of about 2 mm. The actual surface deposits used in our AFM measurements were significantly

denser than those shown in Figure 1c. The average surface number density of the aggregates was about  $10^6/\text{mm}^2$ .

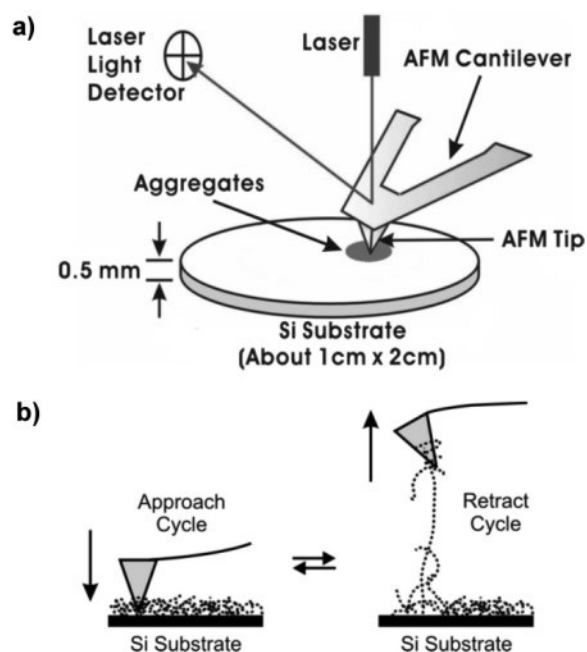
Force measurements were made with an AFM (Bioscope, Veeco Digital Instruments, Santa Barbara) in air at room temperature.  $\text{SiN}_4$  triangular cantilevers with spring constants of 0.06 N/m were used (DNP, Veeco Digital Instruments, Santa Barbara). Force curves were measured at  $5 \mu\text{m/s}$  and analyzed using software we programmed using LabView (National Instruments). To achieve high sensitivity the microscope was housed on a vibration-isolation air table inside an acoustic isolation chamber shielded from electrical noise and thermal drift. The entire system was then placed inside a soundproof room, and all electronics (computers, controllers, pumps) were kept in a separate room. The vertical noise level of the system, determined through standard procedures, was 0.06 nm (RMS).

Recording TEM images necessitated low NCA stretching speeds of  $\sim 0.2 \mu\text{m/s}$ , whereas AFM studies required speeds of  $5 \mu\text{m/s}$  for optimal signal-to-noise ratios. However, AFM measurements in the range of  $0.5\text{--}50 \mu\text{m/s}$  show an expected increase in the observed pulling forces.<sup>26</sup> Nevertheless, no major qualitative differences in the NCA's nanomechanical properties were indicated over this range. Consequently, we chose a pulling speed that optimized signal-to-noise and high resolution to identify individual NCA breaking events. Clearly it would be desirable to combine the observational capability of TEM with the AFM force-displacement measurements in the same online measurement system to study the dynamic properties of NCA.

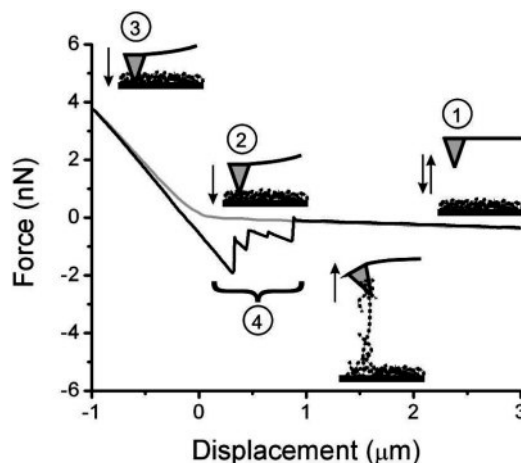
As shown in Figure 2a, the AFM tip is brought into contact with the graphitic aggregate layer on the surface of the silicon substrate. One or several aggregates usually bind nonspecifically to the AFM tip. When the tip is raised, the attached NCAs are pulled up and away from the aggregate deposit on the substrate (Figure 2b). The force and  $z$ -position of the tip above the surface are recorded and statistically analyzed.

Figure 3 shows a typical force curve measured for NCAs deposited on a silicon substrate. The force curve was determined by measuring the deflection of the cantilever as it approached and retracted from the sample. Multiplying the deflection of the cantilever by its spring constant yielded the force acting on the cantilever. During the approach portion of the force curve the net force on the cantilever remained at zero as it neared the surface before it came into contact. A sudden increase in force was observed when the cantilever contacted the surface; at this point the force acting on the cantilever began to monotonically increase as the AFM tip was pushed against the surface. NCAs attached to the tip were then pulled and stretched, deflecting the cantilever downward. (In applications to polymers, it is commonly assumed that the force acts along the polymer perpendicular to the surface.<sup>16</sup> We have made the same assumption in analyzing the stretching and breaking of nanoparticle chains as discussed later.)

Figure 3 shows a typical "sawtooth" profile observed during retraction. We hypothesize that the sawtooth profile corresponds to the stretch and sequential breakage/detachment of single aggregates pulled by the tip which is



**Figure 2.** Schematics of the AFM experiment. (a) The AFM tip is brought into contact with the graphitic aggregate layer on the surface of the silicon substrate. The deflection of the cantilever in response to interactions at the tip changes the reflecting angle of the laser beam striking the cantilever. The angle changes are measured by the laser light detector. We used  $\text{SiN}_4$  triangular cantilevers with spring constants of 0.06 N/m (DNP, Veeco Digital Instruments, Santa Barbara). (b) During the approach period, several graphitic aggregates may become attached to the tip through a network structure and be stretched during the tip retraction.



**Figure 3.** A typical force vs displacement curve recorded as the AFM tip approaches (gray line) and retracts (black line) from an aggregate-coated silicon substrate. The light gray curve represents the force acting on the tip as it moves toward the substrate surface (step 1), at the contact point (step 2), and while it is indented into the sample (step 3). The black line is the force acting on the tip as it moves away from the surface (step 4). On aggregate-coated surfaces, multiple rupture events forming a sawtooth pattern were always observed during the retraction portion of the measurement.

confirmed by TEM observations that two or more chains rarely break at the same time (Figure 1a). We have also captured this behavior on videotape. Other studies<sup>10,11</sup> indicate that the graphitic aggregates break instead of being detached from the substrate during stretching. This behavior

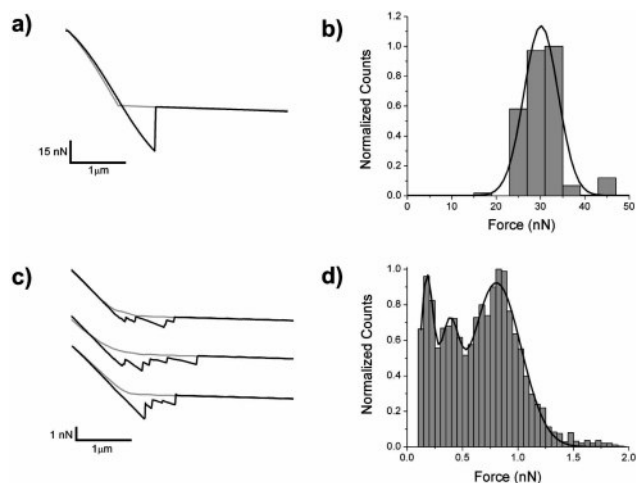


**Figure 4.** Typical force curves and histograms measured on bare silicon and the silicon substrate coated with graphitic aggregates. (a) A typical force curve on bare silicon measured in the same way as the force curve in Figure 3. (b) A histogram of the forces observed in force curves measured on bare silicon in 1300 experiments. The peak in the distribution of forces is at  $30.13 \pm 7.69$  nN. (c) Three typical force curves on the graphitic aggregate surface. (d) A histogram of the forces observed in force curves measured on the graphitic aggregate surface in 1300 experiments. Three populations of forces are seen here at  $0.17 \pm 0.12$  nN,  $0.37 \pm 0.18$  nN, and  $0.80 \pm 0.45$  nN.

has also been observed in previous force spectroscopy studies of DNA<sup>13,14</sup> and proteins;<sup>15–17</sup> the last rupture event is conventionally assumed to be caused by a single molecule. In this case we follow that assumption and attribute the last rupture event to a single chain aggregate.

The force curve in Figure 3 differs clearly from that measured on a clean silicon substrate (Figure 4 a). In Figure 4a, only one rupture event was observed and was reproducible in over 1300 measurements. On average we measured a rupture force of  $30.13 \pm 7.69$  nN (Figure 4b), much higher than the forces observed for the graphitic aggregate measurements shown in Figure 3. This event observed with the clean silicon substrate is due to attraction between the tip and the surface as well as attraction due to a thin film of water at the interface between the cantilever tip and the silicon surface.

We also measured 1300 force curves for NCA deposited on a silicon substrate. A statistical analysis of these data was conducted by measuring the force difference between the bottom and the top of each rupture event and compiling the data into histograms (Figure 4b,d). All measurements were made in 1 day with the same tip in order to rule out artifacts caused by small changes in tip geometry, spring constant, and environmental factors such as humidity and temperature. Gathering a statistically significant number of force curves on the same day with the same tip allows us to make direct comparisons of the data against each other and identify trends in the force characteristics of the stretching/breaking process.

Figure 4c shows three force vs displacement curves randomly picked out of the 1300 experiments. In Figure 4d, the data from 1300 experiments are plotted as a histogram. Peaks were observed in the distributions of forces at  $0.17 \pm 0.12$  nN,  $0.37 \pm 0.18$  nN, and  $0.80 \pm 0.45$  nN. The

mechanisms behind the observed trends are not yet explicitly understood, but these forces may correspond to several processes during the stretching/breaking, such as detachments between aggregates, unfolding and breaking of NCAs. In previous studies,<sup>10,11</sup> we stretched the graphitic NCAs in the TEM, and the NCA broke when the tensile strength was exceeded. Hence the maximum measured force ( $0.80 \pm 0.45$  nN) may correspond to the breaking of NCA. Based on this assumption, we can estimate the tensile strength of the graphitic NCAs as follows.

The tensile strength (TS) is defined as the ratio of the maximum load a body can bear ( $F_{\text{break}}$ ) before breaking to the original cross-sectional area ( $A$ ):

$$TS = \frac{F_{\text{break}}}{A} \quad (1)$$

Assuming the aggregate behaves like a wire with a uniform cross section, the cross section,  $A$ , is

$$A = \frac{\pi d^2}{4} \quad (2)$$

where  $d$  is the average diameter of the primary particles in the aggregates, which can be obtained from the TEM image. Thus,

$$TS = \frac{F_{\text{break}}}{\frac{\pi d^2}{4}} = \frac{4F_{\text{break}}}{\pi d^2} \quad (3)$$

The tensile strength of graphitic NCA is estimated to be about  $4.5 \pm 2.5$  MPa, which is comparable to bulk values (3–10 MPa).<sup>27</sup>

The peaks observed in the distribution of forces at  $0.17 \pm 0.12$  nN and  $0.37 \pm 0.18$  nN may be related to other processes that occur during NCA stretching, such as aggregate detachments and the unfolding of aggregate kinks. The two peaks may correspond to the detaching and unfolding forces as follows. (a) Detaching force. Force is needed to pull one or more aggregates from the network or the agglomerate on the substrate. Agglomerates are assemblies of aggregates held together by weak bonds that may be due to van der Waals forces or ionic/covalent bonds operating over very small contact areas.<sup>2,28</sup> Aggregates are assemblies of primary particles held together by strong bonds, probably ionic/covalent in nature. The two peaks occurring at lower forces in Figure 4d may correspond to the force needed to detach an aggregate from the agglomerate, which requires less force than breaking an aggregate. (b) Unfolding force. Graphitic NCA is an elastic chain, in which force-driven unfolding events occur during stretching.<sup>10,11</sup> Chain kinks on the scale of a few particle diameters are probably straightened by rotation and/or sliding at particle–particle interfaces, which are relatively low-energy processes that lead to large changes in the length of the chain as kinks straighten. The rotation and/or sliding process may be lubricated by the fluidity of the material

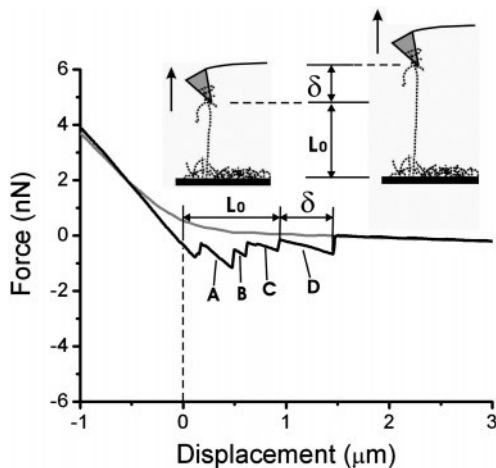


**Figure 5.** Estimation of the Young's modulus of graphitic NCA using the force vs displacement curve. A, B, C, and D indicate the slopes in the curve. The two inset schematics show the stretching situations corresponding to the beginning and the end (right before the chain breaking) of slope D, respectively. The original length ( $L_0$ ) and length change ( $\delta$ ) of the chain are labeled on curves and schematics.

between some of the particles.<sup>10</sup> This process includes overcoming the force of attraction, which may be van der Waals in origin, between neighboring particles on the chain.

There may be other explanations for different force distributions, such as the different primary particle sizes and detailed structures of each NCA. Satisfactory explanation of the histogram in Figure 4d requires better understanding of the structure of graphitic NCAs, the dynamics of aggregates under tension, and the process of chain stretching in the AFM.

As shown in Figure 5, the slope of the curve during stretching, which may be related to the overall elastic constant of the aggregates under tension, decreases gradually from region A to D. This can be explained by the decrease in the number of aggregates stretched as the aggregates break one by one; the last slope, slope D, in the sawtooth region may show the stretching and breaking of the last single chain aggregate and make it possible to estimate the tensile strength and Young's modulus of a single chain aggregate.

The starting point of slope D may correspond to the beginning of stretching of the last attached NCA, as illustrated by the inset schematics in Figure 5. Therefore, the distance between the starting point of slope D and the surface of the substrate can be viewed as the original length ( $L_0$ ) of the last chain. The length change ( $\delta$ ) can be estimated from the displacement of the AFM tip during the chain stretch.

The Young's modulus,  $E$ , of graphitic aggregates can be estimated by dividing the stress,  $\sigma$ , by the strain,  $\epsilon$ , during the stretch of the last single chain. The slope of the last breaking event is constant, consistent with previous TEM studies<sup>11</sup> in which we observed that for small strains the NCA response is elastic. Stress is defined as the product of dividing the applied load,  $F$ , by the specimen's original cross-sectional area,  $A$ . We have

$$\sigma = \frac{F}{A} \quad (4)$$

$F$  can be obtained from the force vs distance curve and  $A$  from eq 2. Strain is calculated by dividing the change in the chain length,  $\delta$ , by the chain's original length  $L_0$ . We have

$$\epsilon = \frac{\delta}{L_0} \quad (5)$$

Using the force vs displacement curves and eq 5, the maximum strain of graphitic NCAs in the experiments can be calculated. The value was about 20–60%, consistent with the results obtained in previous TEM experiments.<sup>11</sup> Therefore, the Young's modulus of the chain

$$E = \frac{\sigma}{\epsilon} = \frac{\frac{F}{A}}{\frac{\delta}{L_0}} = \frac{F}{\delta} \frac{L_0}{A} = \frac{4FL_0}{\pi\delta d^2} \quad (6)$$

where  $F$  is the load applied to the chain,  $L_0$  and  $\delta$  are the original chain length and the change of the chain length, respectively;  $d$  is the primary particle diameter of the graphitic aggregates.  $F$ ,  $L_0$ , and  $\delta$  can be directly obtained from the diagram in Figure 5;  $d$  can be measured from the TEM image of graphitic NCAs. Using eq 6, the Young's modulus of graphitic NCAs was estimated to be in the range of 3.0 to 8.8 MPa, much smaller than the bulk value for graphite (2.1 to 18.6 GPa),<sup>29</sup> indicating the graphitic NCAs are significantly more elastic than bulk graphite. This large difference in values of mechanical properties at the nanoscale has also been observed in other studies, for example, the comparison of the bulk and nanoscale mechanical properties of carbon nanotubes.<sup>30</sup>

In summary, the interaction of an AFM tip with individual chain aggregates of graphitic nanoparticles deposited on a silicon substrate was studied. The forces measured by the cantilever were recorded and statistically analyzed. The characteristic sawtooth pattern was interpreted as a series of stretching/breaking events of the aggregates. Calculated tensile strength ( $4.5 \pm 2.5$  MPa) based on the sawtooth events compares well with the literature value. Estimated values of Young's modulus (3.0 to 8.8 MPa) of single aggregates are significantly lower than literature bulk values. This work reveals a method for determining the nanoscale properties of single NCAs that has not been described previously and that lends insight into the influence of their nanoscale properties on the bulk values of elastomers.

**Acknowledgment.** The authors thank Dr. Martin Seipenbusch for providing the silicon substrates and helpful discussions. W.R. and S.K.F. acknowledge NSF grant CTS 0242026 for partial sponsorship of this research. A.E.P., A.R. and J.K.G. acknowledge partial support from the Institute for Cell Mimetic Space Exploration – CMISE (a NASA URETI Institute).

## References

- (1) Medalia, A. I.; Kraus, G. In *Science and Technology of Rubber*, 2nd ed.; Mark, J. E., Erman, B., Eirich, F. R., Eds.; Academic: New York, 1994.

- (2) Friedlander, S. K. *Smoke, Dust and Haze: Fundamentals of Aerosol Dynamics*, 2nd ed.; Oxford University Press: New York, 2000.
- (3) O'Farrell, C. P.; Gerspacher, M.; Nikiel, L. *Kaut. Gummi Kunst.* **2000**, *53*, 701.
- (4) Medalia, A. I. *Rubber Chem. Technol.* **1986**, *59*, 432.
- (5) Aminabhavi, T. M.; Cassidy, P. E.; Thompson, C. M. *Rubber Chem. Technol.* **1990**, *63*, 451.
- (6) Mark, J. E. *J. Phys. Chem. B* **2003**, *107*, 903–913.
- (7) Friedlander, S. K.; Jang, H. D.; Ryu, K. H. *Appl. Phys. Lett.* **1998**, *72*, 173–175.
- (8) Pu, Z. C.; Mark, J. E.; Jethmalani, J. M.; Ford, W. T. *Chem. Mater.* **1997**, *9*, 2442–2447.
- (9) Suh, Y. J.; Prikhodko, S. V.; Friedlander, S. K. *Microsc. Microanal.* **2002**, *8*, 497.
- (10) Suh, Y. J.; Friedlander, S. K. *J. Appl. Phys.* **2003**, *93*, 3515–3523.
- (11) Bandyopadhyaya, R.; Rong, W. Z.; Friedlander, S. K. *Chem. Mater.* **2004**, *16*, 3147–3154.
- (12) Binnig, G.; Quate, C. F.; Gerber, C. *Phys. Rev. Lett.* **1986**, *56*, 930–933.
- (13) Lee, G. U.; Chrisey, L. A.; Colton, R. J. *Science* **1994**, *266*, 771–773.
- (14) Krautbauer, R.; Schrader, T. E.; Pope, L. H.; Allen, S.; Gaub, H. E. *Biophys. J.* **2002**, *82*, 141a–142a.
- (15) Hugel, T.; Grosholz, M.; Clausen-Schaumann, H.; Pfau, A.; Gaub, H.; Seitz, M. *Macromolecules* **2001**, *34*, 1039–1047.
- (16) Rief, M.; Gautel, M.; Oesterhelt, F.; Fernandez, J. M.; Gaub, H. E. *Science* **1997**, *276*, 1109–1112.
- (17) Li, H. B.; Oberhauser, A. F.; Fowler, S. B.; Clarke, J.; Fernandez, J. M. *Proc. Natl. Acad. Sci. U.S.A.* **2000**, *97*, 6527–6531.
- (18) Garnier, L.; Gauthier-Manuel, B.; van der Vegte, E. W.; Snijders, J.; Hadziioannou, G. *J. Chem. Phys.* **2000**, *113*, 2497–2503.
- (19) Froeschke, S.; Kohler, S.; Weber, A. P.; Kasper, G. *J. Aerosol Sci.* **2003**, *34*, 275–287.
- (20) Lacour, S. P.; Wagner, S.; Huang, Z. Y.; Suo, Z. *Appl. Phys. Lett.* **2003**, *82*, 2404–2406.
- (21) Hsu, P. I.; Huang, M.; Xi, Z.; Wagner, S.; Suo, Z.; Sturm, J. C. *J. Appl. Phys.* **2004**, *95*, 705–712.
- (22) Hsu, P. I.; Huang, M.; Gleskova, H.; Xi, Z.; Suo, Z.; Wagner, S.; Sturm, J. C. *IEEE Trans. Electron. Dev.* **2004**, *51*, 371–377.
- (23) Ullmann, M.; Friedlander, S. K.; Schmidt-ott, A. *J. Nanoparticle Res.* **2002**, *4*, 499–509.
- (24) Ogawa, K.; Vogt, T.; Ullmann, M.; Johnson, S.; Friedlander, S. K. *J. Appl. Phys.* **2000**, *87*, 63.
- (25) Hering, S. V.; Flagan, R. C.; Friedlander, S. K. *Environ. Sci. Technol.* **1978**, *12*, 667–673.
- (26) Strunz, T.; Oroszlan, K.; Schafer, R.; Guntherodt, H. J. *Proc. Natl. Acad. Sci. U.S.A.* **1999**, *96*, 11277–11282.
- (27) Perry, R. H.; Green, D. W. *Perry's Chemical Engineers' Handbook*, 7th ed.; McGraw-Hill: New York, 1997.
- (28) Bandyopadhyaya, R.; Lall, A. A.; Friedlander, S. K. *Powder Technol.* **2004**, *139*, 193–199.
- (29) Lynch, C. T. *Practical Handbook of Materials Science*; CRC Press: Boca Raton, 1989.
- (30) Dalton, A. B.; Collins, S.; Razal, J.; Munoz, E.; Ebron, V. H.; Kim, B. G.; Coleman, J. N.; Ferraris, J. P.; Baughman, R. H. *J. Mater. Chem.* **2004**, *14*, 1–3.

NL0487368